Springer Proceedings in Physics 1068

Ching Yern Chee
Cong Wang *Editors*

Proceedings of the 7th International Conference on Materials Engineering and Nanotechnology 2023 (ICMEN 2023); 04-05 Nov, Kuala Lumpur, Malaysia

Innovative Approach and Recent Developments in Materials Engineering & Nanotechnology

Springer

Springer Proceedings in Physics **1068**

Indexed by Scopus

The series Springer Proceedings in Physics, founded in 1984, is devoted to timely reports of state-of-the-art developments in physics and related sciences. Typically based on material presented at conferences, workshops and similar scientific meetings, volumes published in this series will constitute a comprehensive up to date source of reference on a field or subfield of relevance in contemporary physics. Proposals must include the following:

- Name, place and date of the scientific meeting
- A link to the committees (local organization, international advisors etc.)
- Scientific description of the meeting
- List of invited/plenary speakers
- An estimate of the planned proceedings book parameters (number of pages/articles, requested number of bulk copies, submission deadline).

Please contact:

For Americas and Europe: Dr. Zachary Evenson; zachary.evenson@springer.com
For Asia, Australia and New Zealand: Dr. Loyola DSilva; loyola.dsilva@springer.com

Ching Yern Chee · Cong Wang
Editors

Proceedings of the 7th International Conference on Materials Engineering and Nanotechnology 2023 (ICMEN 2023); 04-05 Nov, Kuala Lumpur, Malaysia

Innovative Approach and Recent Developments in Materials Engineering & Nanotechnology

Springer

Editors
Ching Yern Chee
Faculty of Engineering
Universiti Malaya
Kuala Lumpur, Malaysia

Cong Wang
School of Integrated Circuit Science
and Engineering
Beihang University
Beijing, China

ISSN 0930-8989 ISSN 1867-4941 (electronic)
Springer Proceedings in Physics
ISBN 978-981-97-4079-6 ISBN 978-981-97-4080-2 (eBook)
https://doi.org/10.1007/978-981-97-4080-2

This Springer imprint is published by the registered company Springer Nature Singapore Pte Ltd.
The registered company address is: 152 Beach Road, #21-01/04 Gateway East, Singapore 189721, Singapore

Contents

Analysis of the Heat Transfer and Fluid Flow of SiO_2-Water Nanofluids in the Shell Side of a Shell-and-Tube Heat Exchanger Using Computational Fluid Dynamics

Ethan Zachary G. Castro[1,2(✉)], Allan N. Soriano[3], and Bonifacio T. Doma Jr.[1,2]

[1] School of Chemical, Biological, and Materials Engineering and Sciences, Mapúa University, 1002 Muralla Street, Intramuros, Manila, Philippines
ezgcastro@mymail.mapua.edu.ph

[2] School of Graduate Studies, Mapúa University, 1002 Muralla Street, Intramuros, Manila, Philippines

[3] Chemical Engineering Department, Gokongwei College of Engineering, De La Salle University, 2401 Taft Avenue, Manila, Philippines

Abstract. In response to the imperatives of energy optimization in industrial processes, this research endeavors to examine the potential of SiO_2-water nanofluids as heat transfer media within shell and tube heat exchangers. Employing Computational Fluid Dynamics (CFD) simulations using ANSYS Fluent 2023 R1, a comprehensive analysis is conducted, encompassing nanofluid concentrations spanning 0.1% to 1.0% by volume and turbulence regimes across Reynolds numbers ranging from 20,000 to 83,000. The results consistently demonstrate a positive correlation between heat transfer enhancement and particle loading, culminating in a notable 2.1% augmentation in heat transfer coefficient at the highest particle loading and turbulence level under investigation. Notably, the associated escalation in pressure drop, while present, remains relatively modest in comparison to other nanofluids in similar studies. In order to facilitate the practical application of these findings, the introduction of a performance index, representing the ratio of heat transfer enhancement to pressure drop increase, serves as a critical cost-benefit metric. This index highlights that optimal operational conditions for the utilization of SiO_2-water nanofluids as coolants in heat exchangers are situated within lower turbulent regimes and particle loading ranges. Ultimately, the study underscores the need to balance the enhancement of heat transfer with the management of pressure drop in such applications.

Keywords: SiO_2-water Nanofluid · Computational Fluid Dynamics · Performance index · Shell and tube heat exchanger · ANSYS Fluent

1 Introduction

Rising energy costs necessitate energy optimization in industrial processes. Because of this, a field of research emerged aimed at optimizing or improving the transfer of energy in heat transfer processes. Both active and passive methods were used and studied, with

C. Y. Chee and C. Wang (Eds.): ICMEN 2023, SPPHY 1068, pp. 1–19, 2024.
https://doi.org/10.1007/978-981-97-4080-2_1

the passive ones being more favorable as they are simpler to implement and do not require external forces. One passive method of improving heat transfer is dissolving particles into base heat transfer fluids. In 1904, Maxwell pioneered the development of methods aiming to improve fluid transport properties by suspending millimeter to micrometer-sized solid particles [1]. However, due to the relatively large size of the particles, the pressure drop significantly increased, thus hindering the application. This led to engineering nanoparticles into base fluids such as water to enhance their heat transfer properties [2].

The early 21st century has seen studies on heat transfer applications of nanofluids being focused on how heat transfer enhancement occurs and to what extent heat transfer properties are improved [3–5]. It was established that the enhancement in heat transfer capabilities could be primarily attributed to the contribution of relatively high thermal conductivity nanoparticles, particularly metallic oxide nanoparticles, partnered with increased flow turbulence due to the dispersion of the nanoparticles [6]. Heat transfer coefficient enhancements of up to 30% have been recorded [2]. In the current decade, studies in this area shifted to balancing the heat transfer enhancement against the pressure drop. This is necessary for this technology to be used in industrial and commercial applications. For example, Zhang et al. [7] and Cruz et al. [8] utilized a thermal performance index in their heat transfer performance analyses, which is a ratio of the heat transfer enhancement to the pressure drop enhancement, with values greater than unity being feasible. Hamid et al. [9] investigated the performance of water-based nanofluids containing varying mixture ratios of TiO_2 and SiO_2, as SiO_2 is known to cause milder increases in pressure drop compared to other metallic oxide nanoparticles. Further, numerical analyses such as Computational Fluid Dynamics are being used instead of traditional pilot-scale experiments to address the issue of nanofluids being unstable, especially in low concentrations. Numerical simulations also allow researchers to study the thermal and flow profile of the nanofluid across the entire domain, in contrast to actual experiments where data points may be limited. This also allows flexibility in the flow system geometry and design, as was demonstrated in the study of Ding et al. [10], where they compared the performance of TiO_2-water nanofluid in a corrugated and smooth shell and tube heat exchanger. However, using simulation techniques has its drawbacks, the most notable of which are the assumptions applied to conserve computational power. The single-phase, Newtonian fluid model is the most commonly used approximation to describe the flow properties of the nanofluids in simulation studies. Klazly et al. [11] compared the results of using this conventional model with non-Newtonian and two-phase models. They found that the Newtonian model overestimated the heat transfer coefficient, while the single-phase model underestimated it. Meanwhile, the model of Zhang et al. [7] employing the conventional model severely underestimated the pressure drop. That being said, until more realistic models are available, the results of simulation studies are best used to study trends and patterns rather than taking the exact values for what they are.

Despite the swift progress of the state of the art, there is a lack of parameter studies on the performance of nanofluids as heat transfer fluids. Further, to our best knowledge, most of the available parameter studies only deal with heat transfer enhancement and fail to account for the increase in pressure drop. Given this, the main objective of this

research is to analyze the effects of varying the flow rate and the volume concentration on the performance index of the SiO_2-water nanofluid system by using it as a heat transfer fluid in a simulated miniature shell and tube heat exchanger. The performance index, defined as the ratio of heat transfer enhancement to that of the pressure drop increase, serves as a cost-benefit analysis to determine feasible operating conditions. The primary significance of this study lies with the incorporation of pressure drop effects to the performance analyses of nanofluids as heat transfer fluids. From an economic point of view, the pressure drop is as important as the heat transfer rate since continuous flow of fluids is desired in setups such as heat exchangers. In this regard, the optimization of the heat transfer rate must go hand-in-hand with the minimization of pressure drop, which is why the performance index is used to evaluate the overall feasibility of employing nanofluids in systems such as heat exchangers. Knowing the factors and how they affect both heat transfer and pressure drop is necessary to balance the benefits against the cost, which is vital for the industrial application of this technology.

2 Methodology

Any computational fluid dynamics analysis comprises three steps: pre-processing, processing, and post-processing [8]. In the first step, the geometry and mesh of the domains are defined. The processing stage, meanwhile, involves the definition of the governing equations, numerical models, materials, and the boundary conditions of the given problem. The results are then viewed and analyzed in the post-processing stage. All the steps were done in ANSYS 2023 R1.

2.1 Pre-processing

The geometry model used was adapted from the work of Cruz et al. [8], who have adapted their model from Ozden and Tari [12]. The three-dimensional model of the shell and tube heat exchanger was drawn using ANSYS DesignModeler. Figure 1 shows the heat exchanger geometry constructed, while the specifications are listed in Table 1. The nanofluid is allocated in the shell side of the shell and tube heat exchanger. The tubes were constructed as heated solid cylinders. The ANSYS material database was used for the material specifications, in which aluminum was used as the material for the tube pipes, the shell casing, and the baffles.

The meshing was done using ICEM CFD. An element size of 325 mm was specified, and the mesh ended up with 159,267 nodes and 494,094 elements, with the skewness in both the fluid domain and the tubes minimized. Figure 2 exhibits the mesh along the length of the fluid domain inside the heat exchanger.

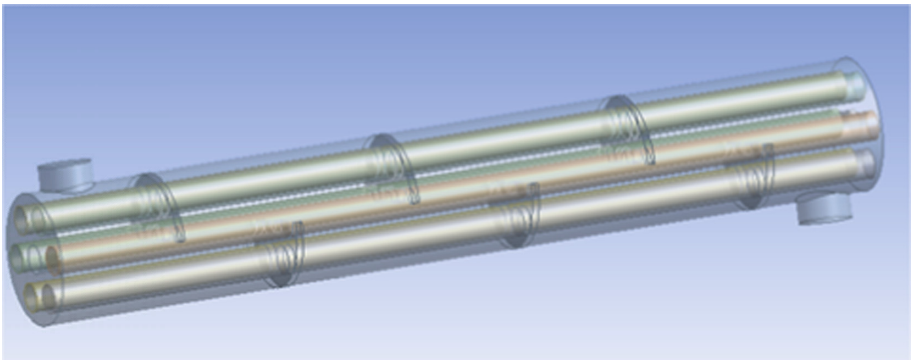

Fig. 1. Heat exchanger geometry

Table 1. Heat exchanger geometry specifications [12]

Parameters	Dimensions
Length	600 mm
Tube Diameter	20 mm
Shell Diameter	90 mm
Number of Tubes	7
Number of Baffles	6
Baffle Spacing	86 mm
Pitch	Triangular, 30 mm
Nozzle Diameter	36 mm

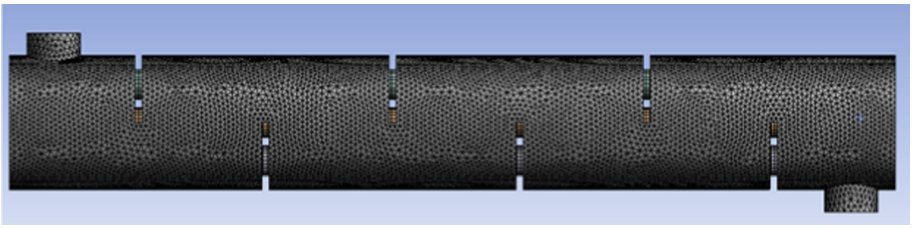

Fig. 2. Mesh along the length of the heat exchanger

2.2 Processing

Steady-state transport is assumed in all the simulations. Equations (1), (2), (3), (4) and (5) are the governing equations for the mass, momentum, and energy conservation in the cylindrical coordinate system. A viscous dissipation function (φ) in cylindrical

coordinates, as shown in Eq. (6), was also incorporated in the energy balance equation.

$$\frac{1}{\mathrm{r}}\frac{\partial(\rho r u_r)}{\partial \mathrm{r}} + \frac{1}{\mathrm{r}}\frac{\partial\left(\rho u_\theta\right)}{\partial \theta} + \frac{\partial(\rho u_z)}{\partial \mathrm{z}} = 0 \tag{1}$$

$$\rho\left(u_r\frac{\partial u_r}{\partial r} + \frac{u_\theta}{r}\frac{\partial u_r}{\partial \theta} + u_z\frac{\partial u_r}{\partial z} - \frac{u_\theta^2}{r}\right) = -\frac{\partial p}{\partial r} + \mu\left[\frac{1}{r}\frac{\partial}{\partial r}\left(r\frac{\partial u_r}{\partial r}\right) + \frac{1}{r^2}\frac{\partial^2 u_r}{\partial \theta^2} + \frac{\partial^2 u_r}{\partial z^2} - \frac{u_r}{r^2} - \frac{2}{r^2}\frac{\partial u_\theta}{\partial \theta}\right] \tag{2}$$

$$\rho\left(u_r\frac{\partial u_\theta}{\partial r} + \frac{u_\theta}{r}\frac{\partial u_\theta}{\partial \theta} + u_z\frac{\partial u_\theta}{\partial z} + \frac{u_r u_\theta}{r}\right) = -\frac{1}{r}\frac{\partial p}{\partial \theta} + \mu\left[\frac{1}{r}\frac{\partial}{\partial r}\left(r\frac{\partial u_\theta}{\partial r}\right) + \frac{1}{r^2}\frac{\partial^2 u_\theta}{\partial \theta^2} + \frac{\partial^2 u_\theta}{\partial z^2} + \frac{2}{r^2}\frac{\partial u_r}{\partial \theta} - \frac{u_\theta}{r^2}\right] \tag{3}$$

$$\rho\left(u_r\frac{\partial u_z}{\partial r} + \frac{u_\theta}{r}\frac{\partial u_z}{\partial \theta} + u_z\frac{\partial u_z}{\partial z}\right) = -\frac{\partial p}{\partial z} + \mu\left[\frac{1}{r}\frac{\partial}{\partial r}\left(r\frac{\partial u_z}{\partial r}\right) + \frac{1}{r^2}\frac{\partial^2 u_z}{\partial \theta^2} + \frac{\partial^2 u_z}{\partial z^2}\right] + \rho g_z \tag{4}$$

$$\nabla(\rho e\vec{u}) = -p\nabla(u) + \nabla(k\nabla T) + q + \Phi \tag{5}$$

$$\Phi = 2\left(\frac{\partial u_r}{\partial r}\right)^2 + 2\left(\frac{1}{r}\frac{\partial u_\theta}{\partial \theta} + \frac{u_r}{r}\right)^2 + 2\left(\frac{\partial u_z}{\partial z}\right)^2 + \left(\frac{\partial u_\theta}{\partial r} - \frac{u_\theta}{r} + \frac{1}{r}\frac{\partial u_r}{\partial \theta}\right)^2 + \left(\frac{1}{r}\frac{\partial u_z}{\partial \theta} + \frac{\partial u_\theta}{\partial z}\right)^2 + \left(\frac{\partial u_r}{\partial z} + \frac{\partial u_z}{\partial r}\right)^2 \tag{6}$$

The turbulence model used in this study was the realizable k-ε model with scalable wall functions. The equations describing the realizable k-ε model a given in Eqs. (7) and (8), with the constants tabulated in Table 2.

$$\frac{\delta}{\delta x_j}(\rho\varepsilon u_j) = \frac{\delta}{\delta j}\left[\left(\mu + \frac{\mu_t}{\sigma_\varepsilon}\right)\frac{\delta\varepsilon}{\delta x_j}\right] + \rho C_1 S\varepsilon + C_{1\varepsilon}\left(\frac{\varepsilon}{k}\right)C_{3\varepsilon}G_b - C_2\rho\left(\frac{\varepsilon^2}{k + \sqrt{\varepsilon v}}\right) + C_\varepsilon \tag{7}$$

$$\mu_t = \frac{\rho C_\mu k^2}{\varepsilon} \tag{8}$$

Table 2. Realizable k-ε model constants

Constants	Value
C1ε	1.44
C_2	1.9
σ_k	1.0
σε	1.2
Cμ	0.09

The second-order spatial discretization scheme was selected for pressure, momentum, turbulent kinetic energy, energy conservation, and dissipation rate. Pressure-velocity coupling was set to coupled, and the temperature limits were set from 300 K (inlet) to 450 K (outlet). The convergence criteria were set at 10^{-6} residuals for the energy conservation equation and 10^{-3} residuals for everything else, or 1000 iterations, whichever finished first.

2.3 Fluid Properties

The nanofluid is assumed to be Newtonian. The flow behavior of the nanoparticles and the base fluid (water) is assumed to be completely fluidized in the heat exchanger. The single-phase approximation is valid since only low particle loadings were considered, with a maximum volume fraction of 0.01. The properties introduced to the system were assumed to be independent of temperature and were taken from a reference temperature equal to the inlet temperature of 300 K, except for the thermal conductivity. The variation of the thermal conductivity with temperature was defined using a piecewise-linear function. For this, eleven temperature data points were input to the ANSYS Fluent Solver, ranging from 300 K to 350 K with an increment of 5 K. Table 3 shows the constant properties of water at 300 K, obtained from tables provided by Green and Perry [13].

Table 3. Properties of water at 300 K and atmospheric pressure [13]

Property	Value
Density	997.01 kg per m^3
Viscosity	0.000855 Pa•s
Heat Capacity	4.179 kJ per kg•K

As for the nanofluid properties, the SiO_2-water nanofluids were introduced as homogeneous fluids defined by their effective parameters in terms of their particle loading. The solid SiO_2 nanoparticles were assumed to have a constant density of 2400 kg m^{-3}, a heat capacity of 730 J kg^{-1} K^{-1}, and thermal conductivity of 1.3 W m^{-1} K^{-1} [13]. Equations (9) and (10) were then used to calculate the effective density (ρ_{eff}) and specific heat capacity (Cp_{eff}) at different volume fractions. Ithe equations shown, ρ_{np} is the density of the nanoparticle, φ is the volume fraction, and ρ_{bf} is the density of water.

$$\rho_{eff} = \phi\rho_{np} + (1-\phi)\rho_{bf} \tag{9}$$

$$C_{p_{eff}}\rho_{eff} = \phi\rho_{np}C_{p_{np}} + (1-\phi)\rho_{bf}C_{p_{bf}} \tag{10}$$

The Einstein viscosity model was used to describe the effective viscosity of the SiO_2-water nanofluids, as used in the study of Fazeli et al. [14] in employing SiO_2-water nanofluids in heat sinks. This viscosity model may be considered valid for dilute solutions of SiO_2 in water. Equation (11) exhibits the Einstein viscosity model, where μ_{eff} is the effective viscosity, μ_{bf} is the base fluid viscosity, and φ is the volume fraction or particle loading.

$$\mu_{eff} = \mu_{bf}(1 + 2.5\phi) \tag{11}$$

Meanwhile, Eq. (12) exhibits the thermal conductivity equation used in this study, proposed by Hamilton and Crosser [15]. Initially, this model was used to describe mixtures containing micrometer-sized particles, but the work of Zhang et al. [16] has shown

that the correlation can be extended to nanometer-sized particles as well. The model considers the contribution of the thermal conductivity of the nanoparticle and the base fluid, as well as the volume fraction of nanofluids used, proving to be convenient in the attainment of the objectives of this study.

$$k_{eff} = k_{bf}\left[\frac{k_p + 2k_{bf} - 2\phi\left(k_{bf} - k_p\right)}{k_p + 2k_{bf} + \phi\left(k_{bf} - k_p\right)}\right] \tag{12}$$

2.4 Boundary Conditions

No-slip boundary condition was set at the inner wall of the shell, a the shell side was assumed to be perfectly insulated. Table 4 exhibits a summary of the boundary conditions used. Velocity inlet was set to be the boundary input for the inlet nozzle, so the mass flow rates were manually converted to the corresponding velocity value.

Table 4. Boundary conditions

Conditions	Value
Outlet Gauge Pressure	0
Inlet Temperature	300 K
Hot Tubes Temperature	450 K
Flow Rate (kg per s)	0.50, 1.00, 2.00

2.5 Model Validation

The current model was validated by employing water as the shell side fluid in the simulated shell and tube heat exchanger. The preliminary water simulation used all three inlet mass flow rates. The shell outlet temperature and pressure drop of the water simulations were then compared to the results of the verified work of Ozden and Tari [12], also employing water as the coolant. Once the values agreed to an acceptable extent, the nanofluid simulations were commenced.

2.6 Variation of Parameters

This study was conducted with varying particle loading and mass flow rate. The volume fraction of the nanofluids was varied from 0.10%, 0.25%, 0.50%, and 1.00%. Each particle loading was then subjected to a velocity corresponding to the Reynolds number of water at atmospheric pressure, 300 K, and mass flow rate of 0.5, 1.0, and 2.0 kg per second. The corresponding velocities of the nanofluids were then calculated using Eq. (13), and the resulting inlet velocities are summarized in Table 5. In the equation, u is the inlet velocity, μ is the effective viscosity of the nanofluids, RE denotes the Reynolds

number, D is the inlet nozzle diameter, and ρ is the effective density of the nanofluids. Since correlations on heat transfer coefficients vary directly with the Reynolds number, it is convenient to have this as an independent variable to evaluate the heat transfer enhancement accurately.

Table 5. Inlet velocities (m s^{-1}) of nanofluid at varying Reynolds number and loading

Loading	Reynolds Number		
	20,683	**41,366**	**82,732**
0.10% Volume	0.4932	0.98_{65}	1.97_{29}
0.25% Volume	0.4940	0.98_{80}	1.97_{61}
0.50% Volume	0.49_{54}	0.9907	1.98
1.00% Volume	0.49_{80}	0.99_{60}	1.99

$$u = \frac{\mu R_E}{D\rho} \tag{13}$$

2.7 Post Processing

The ANSYS Fluent Solver Package automatically reports the fluxes and surface area integrals after simulations based on the input conditions. The parameters taken directly from CFD Post, the post-processing client of ANSYS, we the heat transfer rate, outlet temperature, and the static pressure. The pressure drop is then manually calculated as the difference between the static pressures in the inlet and outlet. Next, the heat transfer coefficient was calculated using Eq. (14). In the equation, h is the heat transfer coefficient, Q is the total heat transfer rate, n is the number of tubes, D is the diameter of the tubes, L is the length of the heat exchanger, T_{wall} is the wall temperature of the tubes, and T_{bulk} is the bulk temperature of the coolant.

$$h = \frac{Q}{n\pi DL(T_{wall} - T_{bulk})} \tag{14}$$

The bulk temperature was calculated manually as the average of the inlet and outlet temperatures. The heat transfer coefficient for each run was then manually evaluated from there. After evaluating the heat transfer coefficient, the performance index (η) was computed. Cruz et al. [8] calculated the index by obtaining the ratio of the heat transfer improvement to the pressure drop improvement, as shown in Eq. (15). The higher the value, the more the nanofluid becomes feasible as aeat transfer fluid. This index also serves as the main criterion for determining the extent of the effects of the particle loading and flow rate on heat transfer and flow characteristics of the nanofluid. It may be considered a cost-benefit analysis to determine whether employing the studied

nanofluids will be more feasible than using only water as the coolant in a shell and tube heat exchanger.

$$\eta = \frac{\frac{h_{nf}}{h_{bf}}}{\frac{\Delta P_{nf}}{\Delta P_{bf}}} \tag{15}$$

Aside from the numerical data obtained, the temperature, pressure, and velocity profile of the best-performing nanofluid run was also analyzed as a representative of all nanofluid runs. This was done to point out what exactly happens to the flow and heat transfer behavior as the fluid flows through the shell of the shell and tube heat exchanger.

3 Results and Discussion

3.1 Validation of the Computational Fluid Dynamics (CFD) Model

In this study, verification was done by comparing the shell outlet temperature and pressure drop results to that from the validated model of Ozden and Tari [12]. The outlet temperature data from both studies are summarized in Table 6. The percent error values in the outlet temperature are almost consistent at approximately 5% for all turbulence levels. The highest deviation was observed in the highest turbulence region simulated, under-predicting the shell outlet temperature from the reference model by a magnitude of 18.1 K. The errors incurred can be attributed to the vast difference in the meshing of the current model since the reference model had finer mesh statistics. Thus, more data points were available, and the output values may differ. Nonetheless, the error values incurred were within an acceptable range, confirming the validity of the current model.

Table 6. Validation results using the shell outlet temperature (in K)

Reynolds Number	Current Model	Ozden and Tari [12]	Percentage Error (%)
20,683	319.1	334.2	−4.51%
41,366	312.5	327.7	−4.65%
82,732	307.6	325.7	−5.56%

On the other hand, the current model consistently under-predicted the pressure drop values of the model of Ozden and Tari [12] by approximately 12% at all turbulence regions, as shown in Table 7. Cruz et al. [8], who conducted a similar study with CuO-water nanofluids, also encountered a high percentage difference for the pressure drop with respect to the data of Ozden and Tari [12]. The highest pressure drop percentage difference incurred by their model was 20.72%. This difference again has something to do with the difference in the meshing of the current model and the reference model. The reference model, having more nodes and elements, focused the elements on the walls of the tube and shell and the baffles, thereby obtaining more data points from there. This implies that their pressure drop evaluation considered both form and skin friction

during flow. Meanwhile, the current model focused the elements only on the wall regions, using face and body selection. This means that the current model only accounted for the skin friction, and the friction due to the redirection of flow by the baffles was not fully accounted for. In addition, unspecified measurements such as the distance of the nozzle from the face of the heat exchanger and the baffle thickness, may have also caused some deviations. However, these discrepancies can be justified because the current study aims to determine the performance index and not solely the pressure drop value. The performance index concerns the ratio between the pressure drop of the enhanced fluid to that of the base fluid. Therefore, any discrepancy concerning the pressure drop value is already disregarded when the division operation is performed, considering that the ratio of the differences in the pressure drop of the current and reference models are equal to that of the pressure drop values from the current model.

Table 7. Validation results using pressure drop (in Pa)

Reynolds Number	Current Model	Ozden and Tari [12]	Percentage Error (%)
20,683	1330	1509	−11.86%
41,366	5339	6112	−12.65%
82,732	21464	24464	−12.26%

3.2 Heat Transfer Enhancement

The heat transfer enhancement brought about by suspending SiO_2 nanoparticles in water as coolant in a shell and tube heat exchanger may be directly observed with the effect in heat transfer coefficient since the heat transfer rate is directly proportional to the heat transfer coefficient. With this, Fig. 3 exhibits the percentage of heat transfer coefficient enhancement for SiO_2-water nanofluids at varying particle loading and Reynolds number.

The increase in convective heat transfer coefficient increases with particle loading. This is so because the effective thermal conductivity of the nanofluid increases with increasing particle loading, following the thermal conductivity correlation prescribed by Zhang et al. [16]. A particle loading of 0.10% by volume improved the heat transfer coefficient by approximately 0.7% to 1.8% across all Reynolds numbers simulated. The highest heat transfer coefficient enhancement observed was approximately 2.1%, occurring at 1.00% by volume particle loading and 20,683 Reynolds number. It should be noted, however, that the heat transfer enhancement is observed to decrease with increasing turbulence. This observation implies that employing nanofluids is more effective at lower turbulence regions. A possible explanation for this might be because the fluid having a low Reynolds number flows at a lower velocity in the shell side of the shell and tube heat exchanger. Consequently, the coolant has more residence time inside the shell, allowing for more contact time with the process fluid for heat transfer. These observations stated were consistent with the results of Cruz et al. [8]. In the work of

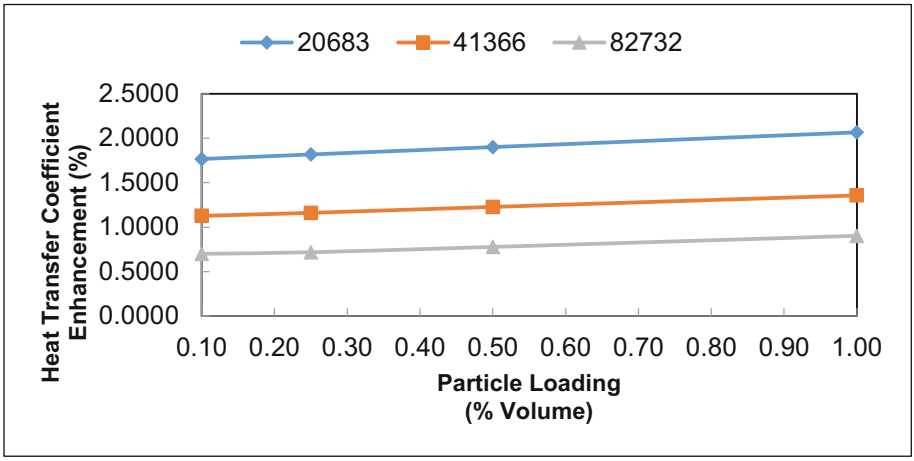

Fig. 3. Heat transfer coefficient enhancement by SiO_2-water nanofluid at varying loading and Reynolds number

Pantzali et al. [17], where CuO-water nanofluids were applied in a miniature plate heat exchanger, the same trend holds. This study found that enhancement in heat transfer properties is more pronounced at lower nanofluid turbulence regions. At higher turbulence, convective heat transfer dominates, and the contribution of the nanoparticle to the fluid heat transfer becomes negligible. This implies that for a given amount of heat duty, the flow rate required for a nanofluid will be lower than that if water was used as the coolant, as nanofluids seem to operate best at lower flow rates.

For the heat transfer behavior of the nanofluids, nothing unusual was observed in the simulations. In all nanofluid simulation runs, the first uniform increase in fluid bulk temperature occurs just after the fourth baffle. In Fig. 4, this is seen as the sudden change in the shade of blue. Further analysis reveals that the heating of the coolant nanofluid commences primarily from the center and then goes outwards, as shown in Fig. 5. The same was also observed in the study of Cruz et al. [8]. Since the heat transfer behavior of the nanofluid is highly similar to that of the base fluid, the most probable main reason for heat transfer is the enhancement in the heat transfer properties of the base fluid.

3.3 Pressure Drop Enhancement

While it was shown in the previous section that using higher particle loading will increase the heat transfer coefficient enhancement, the drawback of using higher loadings is the rise in head losses. The pressure gradient is the driving force of fluid flow, and pressure drop accounts for losses incurred along the flow. Thus, increased pressure drop means a lower pressure gradient and inefficient flow. Figure 6 shows the pressure drop incurred using SiO_2-water nanofluids as coolants in a shell and tube heat exchanger at varying concentrations and Reynolds numbers. The general trend is that the value for the pressure drop increases with increasing particle concentration and turbulence. The effect of nanofluids increasing the pressure drop is brought about by what is known as the viscous effect, where the viscosity of the base fluid increases upon the addition of

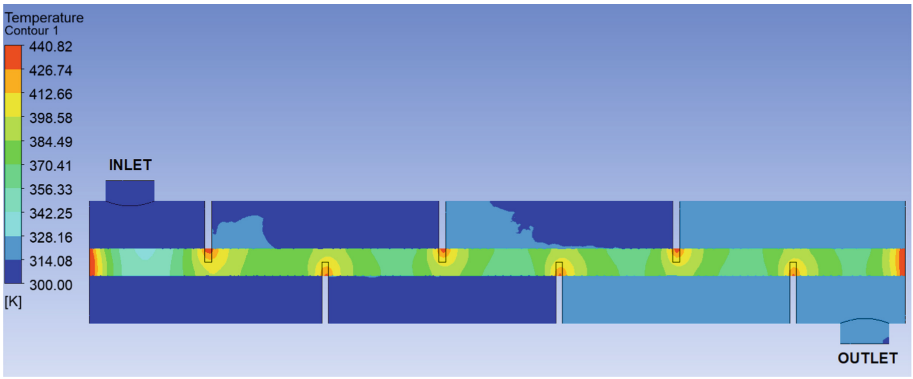

Fig. 4. Temperature contour for SiO_2-water nanofluid at 0.10% particle loading and 20,683 Reynolds number

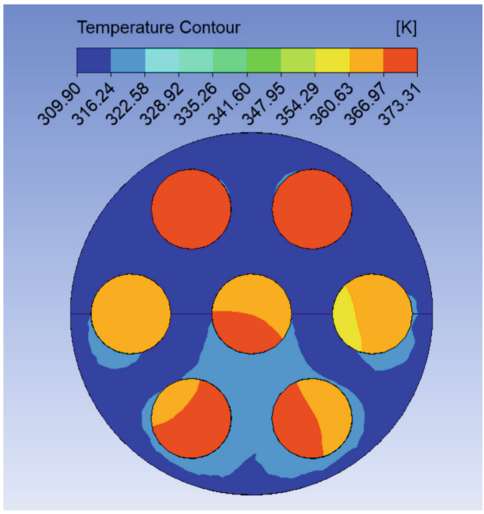

Fig. 5. Cross-sectional temperature contour for SiO_2-water 400 mm along the length at 0.10% loading and 20,683 Reynolds number

solid particles into it. This is because suspending spherical solid particles increases the effect of the drag, the force acting opposite to the relative motion of the fluid as dictated by Newton's Third Law of Motion. Drag force can exist between two fluid layers or between a fluid and a solid layer. In employing nanofluids, the drag comes from both the fluid-fluid and solid-fluid contact, increasing drag effects. Meanwhile, pressure drop increases with increasing turbulence because, as stated, friction is also caused by fluid-fluid contact, and increasing the flow rate shall increase the effects of skin friction. Also, according to the Hagen-Poiseuille Law, the pressure drop is directly proportional to the flow rate [18].

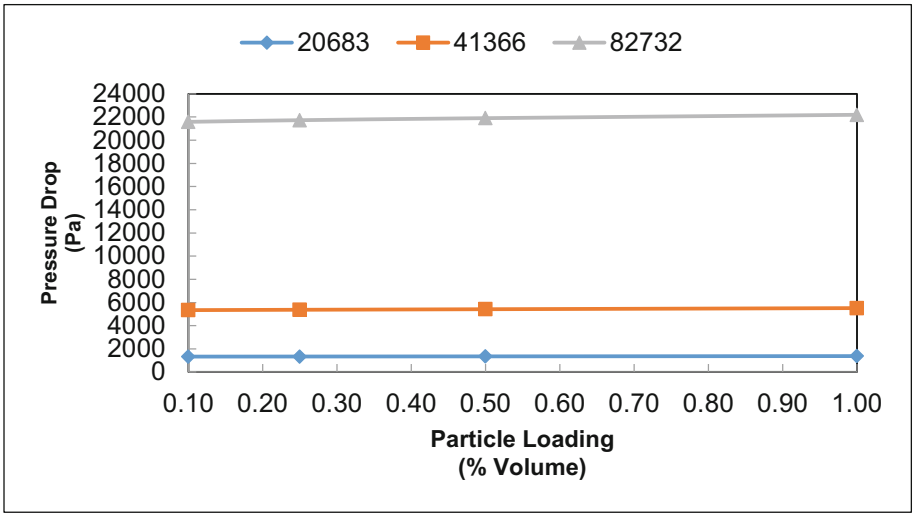

Fig. 6. Pressure drop by using SiO_2 nanoparticles in water at varying loading and Reynolds number

One important observation from the data gathered is that the increase in pressure drop as the particle loading is increased is milder compared to other types of nanofluids simulated in previous studies. This can be seen by the almost horizontal lines when the pressure drop is plotted against the particle loading, as in Fig. 6. No drastic enhancement in the pressure drop was observed when the pressure drop of the SiO_2-water nanofluid was compared with that of water. This may be primarily caused by using only low concentrations of the nanofluid partnered with the Einstein viscosity equation to model the viscosity of the nanofluids. As the maximum volume fraction used in the study is only 0.01, the effective viscosity, according to the Einstein viscosity equation, is essentially the same as that of the base fluid. Other equations modeling the viscosity could have been used. However, the Einstein viscosity equation is considered valid when nanofluid suspensions are dilute, and particle-particle interactions are negligible, both of which are satisfied by the SiO_2-water nanofluid system being studied.

Figure 7 shows the pressure contour generated for the simulation of 0.10% by volume SiO_2-water nanofluid at 20,683 Reynolds number. A smooth pressure gradient can be observed along the length of the heat exchanger, indicative of a relatively low pressure drop. However, just below the inlet, there is a drastic head loss. This was also observed in the work of Rehman [19], where the sudden drop in pressure around the inlet and outlet was associated with fluid impingement at the heat exchanger nozzles. Further analysis by generating the velocity contour and streamline of the same system, shown in Figs. 8 and 9, respectively, revealed an extreme velocity gradient near the inlet nozzle as well. Cruz et al. [8] attribute this to fluid recirculation. In actual application, recirculation zones should be closely monitored, as they contribute to head loss, which is also why an extreme pressure drop is seen at the inlet in almost all nanofluid simulations. Identifying and minimizing fluid recirculation is important to achieve an effective design. Ozden and Tari [12] hypothesized that these recirculation zones, commonly found at inlet nozzles

of flow systems, are due to a boundary layer separation occurring as sudden expansion of fluid occurs. A large pressure gradient at the inlet nozzle is predicted to have caused this. To address this issue, they suggest utilizing other heat exchanger configurations or varying the baffle cut or baffle spacing used in the shell and tube heat exchanger. Also noteworthy from the velocity graphics are the gradients around the baffles. These imply that baffles indeed promote turbulence and aid in maximizing heat transfer. It can also be seen that the local velocity near the inner tube is lower relative to the velocity of the bulk of the fluid, therefore justifying the observations seen from the temperature contour analysis that the heat is concentrated near the center.

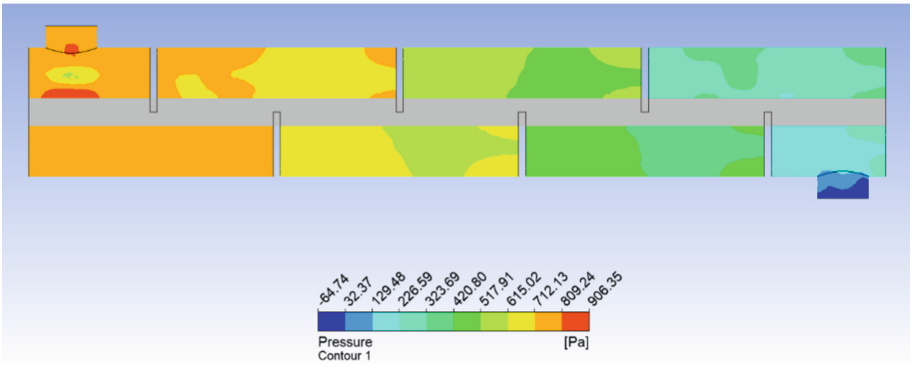

Fig. 7. Pressure contour for 0.10% SiO_2-water at 20,683 Reynolds number

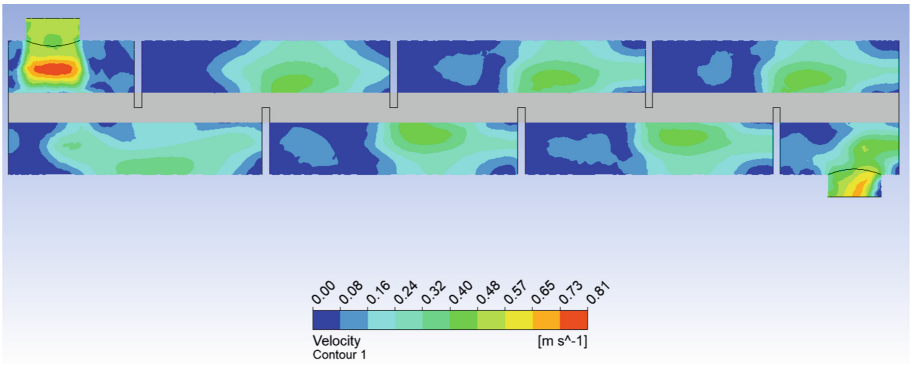

Fig. 8. Velocity contour for 0.10% SiO_2-water at 20,683 Reynolds number

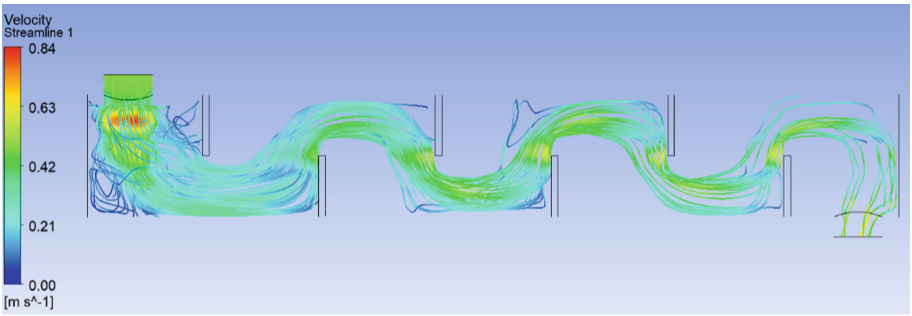

Fig. 9. Velocity streamline for 0.10% SiO_2-water at 20,683 Reynolds number

3.4 Performance Index

The performance index is a measure of the feasibility of using the nanofluid as a heat transfer fluid, as it considers the increase in both the heat transfer and pressure drop. The extent to which pressure drop limits heat transfer can only be emphasized by evaluating the performance indices of each simulation done. Figure 10 shows the performance indices of the SiO_2-water nanofluid at varying particle loading and Reynolds number.

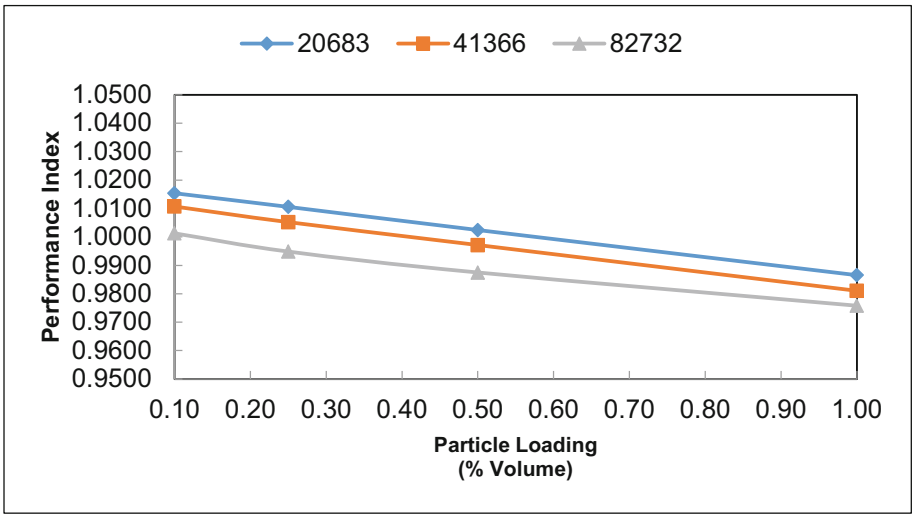

Fig. 10. Performance indices

The performance index decreases with increasing particle loading and turbulence. As expected, since the lowest Reynolds number corresponds to the lowest pressure drop and highest heat transfer enhancements, the highest values for the performance index may be obtained from this turbulence region. The reference value for the performance index is unity, which corresponds to the performance of having only water, the base fluid, as the coolant. This means that a performance index of near unity means that the

increase in pressure drop merely offsets the enhancements to the heat transfer. Moreover, employing conditions with less than unity performance indices would not be feasible, as this means that the undesirable increase in pressure drop is more significant than the desired enhancement in heat transfer. Results of the simulations show that for SiO_2, the conditions that are preliminarily feasible to employ are 0.10% by volume concentration under all flow regimes, 0.25% by volume concentration at Reynolds number 41,366, and 0.50% by volume concentration at Reynolds number 20,683. Emphasis should be made on the term preliminarily feasible since, aside from the heat transfer enhancement and the pressure drop, the actual cost of utilizing such nanoparticles also needs to be considered in choosing which coolant system to use. Though a very significant factor to be considered, the cost of synthesizing and employing the nanoparticles in water for coolant systems is beyond the scope and delimitation of this study. At high concentrations, particularly at the maximum loading considered of 1.00% by volume, the increase in pressure drop is higher relative to the increase in heat transfer, making water as a coolant more feasible. Thus, high particle loadings for SiO_2-water systems may not be advisable for future applications in heat exchange systems. The results of the evaluation of the performance indices of the systems agree with the results of Cruz et al. [8]. In their CuO-water nanofluid simulation, the feasible conditions lie within the lowest turbulent flow regime and the lowest particle loading.

Comparing the performance of the SiO_2-water system to the CuO-water system simulated by Cruz et al. [8], the heat transfer enhancement from SiO_2 was relatively low. The maximum enhancement observed in from the data was 2.1% enhancement in heat transfer coefficient, while for the CuO-water system, a maximum of 48% enhancement was realized. However, Cruz et al. [8] reported that with this enhancement, the pressure drop doubled, drastically affecting the performance index. Figure 11 illustrates the comparison between the performance indices of the SiO_2-water and CuO-water systems at varying loading and Reynolds number of around 20,000. Below 0.35% by volume concentration, the CuO-water system outperforms the SiO_2-water system. This is because CuO has better higher thermal conductivity and lower specific heat capacity than SiO_2. Beyond 0.35%, however, a steep decline in the performance of the CuO-water system can be observed, while the performance of the SiO_2-water system decreases but at a gradual rate. This may be attributed to the slow decrease in pressure drop previously observed for the SiO_2-water system. This makes the SiO_2-water system still feasible to use at around 0.50% loading while the performance index of the CuO-water system is already less than unity at this point. At 1.00% by volume concentration, the CuO-water system is way down in terms of feasibility, while that of the SiO_2-water system is still close to unity. This further emphasizes the need for incorporating the pressure drop in the performance analysis of nanofluids as heat transfer fluids because while the heat transfer enhancement might be high, the increase in head losses may only offset this, or worse, overturn it. The SiO_2-water overall showed minor enhancement in heat transfer but is highly feasible to use according to its performance index values because of its mild pressure drop increase.

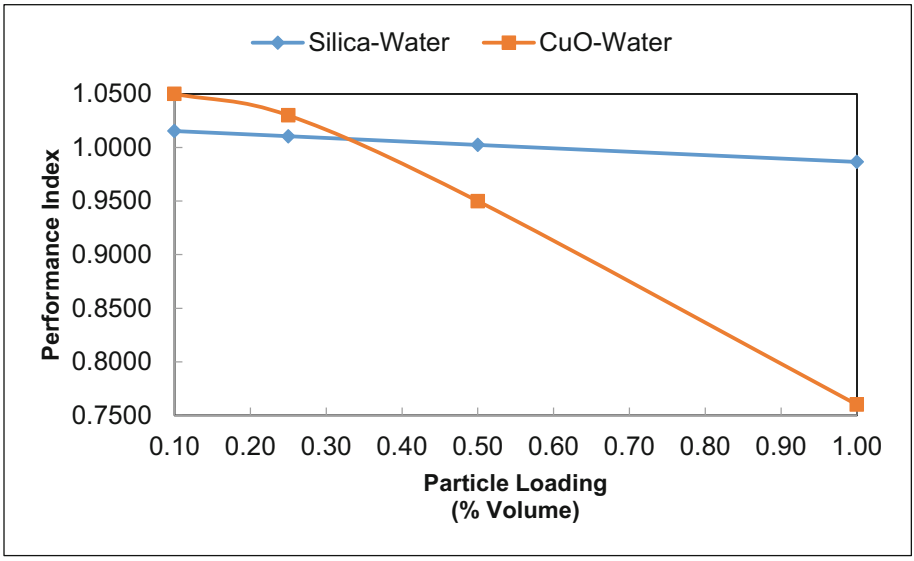

Fig. 11. Performance indices of SiO_2-water and CuO-water [8] nanofluids at 20,000 Reynolds number

4 Conclusion

The Computational Fluid Dynamics (CFD) analysis of the SiO_2-water nanofluids revealed that the heat transfer enhancement and the pressure drop increased with increasing particle loading. However, the heat transfer enhancement decreased with increasing turbulence, mainly because of the faster flow within the shell, implying a shorter residence time for heat transfer. The heat transfer enhancement is mainly attributed to the increase in the effective thermal conductivity and the decrease in the specific heat capacity of the resulting nanofluid, as its heat transfer and flow behavior are highly similar to that of the base fluid. Meanwhile, the pressure drop increase was mainly due to increased drag by suspending spherical solid particles in the fluid. The skin friction during flow increased with the addition of solid-liquid contact friction.

The evaluation of the performance indices shows that the feasible conditions to apply when employing nanoparticles in base fluids for heat transfer were low turbulent regions and low particle loading. A performance index value above unity is desirable since a value of unity means the system is just as effective as using only water as coolant. Consequently, a value of less than unity is not recommended because this implies that only water is much more feasible to use as coolant and that the cost (pressure drop increase) outweighs the benefits (heat transfer enhancement). Results of this study showed that the feasible conditions to apply for the SiO_2-Water system were 0.10% by volume concentration under all flow regimes, 0.25% by volume concentration at Reynolds number 41,366, and 0.50% by volume concentration at Reynolds number 20,683.

Contours were also analyzed to describe the flow and heat transfer behavior of the nanofluid systems. From the temperature contour, it was found that the bulk of the fluid

started increasing in temperature at halfway of the length of the heat exchanger. Cross-sectional analysis of the temperature contour reveals that the heating of the fluid started from the center, near the innermost tube. The velocity contour reveals that the local velocity near the center of the shell was at a minimum, meaning there was a longer residence time of fluid near the innermost tube, maximizing heat transfer. Pressure contours, meanwhile, reveal an intense pressure gradient in all nanofluid runs just below the inlet. Velocity contours reveal that these are zones of recirculation, hypothesized to be due to the boundary layer separation of the fluid upon expansion from the inlet nozzle to the shell.

Overall, for future industrial applications, this study suggests that nanofluids should generally be employed at low turbulent flow regimes and lower particle loading to keep the undesired effects (pressure drop increase) of using nanofluids from outweighing the desired effects (heat transfer enhancement). Depending on the actual cost of procuring such nanofluids, these results may be included in the considerations of which type of heat transfer fluid to use. Also, from the results of the contours, several factors should be monitored in using nanofluids in heat exchangers, such as avoiding recirculation zones at the inlet by monitoring the inlet nozzle pressure and ensuring that the velocity of flow is uniform in all layers to ensure uniform heating of the bulk of the fluid.

References

1. Yu, W., Choi, S.U.S.: The role of interfacial layers in the enhanced thermal conductivity of nanofluids: a renovated maxwell model. J. Nanopart. Res. **5**, 167–171 (2003)
2. Louis, S.P., Ushak, S., Milian, Y., Nemś, M., Nemś, A.: Application of nanofluids in improving the performance of double-pipe heat exchangers—a critical review. Materials **15**(19), 6879 (2022)
3. Maïga, S.E.B., Palm, S.J., Nguyen, C.T., Roy, G., Galanis, N.: Heat transfer enhancement by using nanofluids in forced convection flows. Int. J. Heat Fluid Flow **26**(4), 530–546 (2005)
4. Xuan, Y., Li, Q.: Heat transfer enhancement of nanofluids. Int. J. Heat Fluid Flow **21**(1), 58–64 (2000)
5. Xuan, Y., Roetzel, W.: Conceptions for heat transfer correlation of nanofluids. Int. J. Heat Mass Transf. **43**(19), 3701–3707 (2000)
6. Abdolbaqi, M.K., Azwadi, C.S.N., Mamat, R.: Heat transfer augmentation in the straight channel by using nanofluids. Case Stud. Thermal Eng. **3**, 59–67 (2014)
7. Zhang, S., Li, Lu., Wen, T., Dong, C.: Turbulent heat transfer and flow analysis of hybrid Al2O3-CuO/water nanofluid: An experiment and CFD simulation study. Appl. Thermal Eng. **188**, 116589 (2021)
8. Cruz, P.A.D., Yamat, E.-J.E., Nuqui, J.P.E., Soriano, A.N.: Computational Fluid Dynamics (CFD) analysis of the heat transfer and fluid flow of copper (II) oxide-water nanofluid in a shell and tube heat exchanger. Digit. Chem. Eng. **3**, 100014 (2022)
9. Hamid, K.A., Azmi, W.H., Nabil, M.F., Mamat, R.: Experimental investigation of nanoparticle mixture ratios on TiO2–SiO2 nanofluids heat transfer performance under turbulent flow. Int. J. Heat Mass Transf. **118**, 617–627 (2018)
10. Ding, Z., Qi, C., Luo, T., Wang, Y., Tu, J., Wang, C.: Numerical simulation of nanofluids forced convection in a corrugated double-pipe heat exchanger. Can. J. Chem. Eng. **100**(8), 1954–1964 (2022)

11. Klazly, M., Mahabaleshwar, U.S., Bognár, G.: Comparison of single-phase Newtonian and non-Newtonian nanofluid and two-phase models for convective heat transfer of nanofluid flow in backward-facing step. J. Mol. Liq. **361**, 119607 (2022)
12. Ozden, E., Tari, I.: Shell side CFD analysis of a small shell-and-tube heat exchanger. Energy Convers Manag. **51**(5), 1004–1014 (2010)
13. Green, D., Southard, M.: Perry's Chemical Engineers' Handbook. 8th edn. McGraw Hill (2018)
14. Fazeli, S.A., Hosseini Hashemi, S.M., Zirakzadeh, H., Ashjaee, M.: Experimental and numerical investigation of heat transfer in a miniature heat sink utilizing silica nanofluid. Superlattices Microstruct. **51**(2), 247–264 (2012)
15. Hamilton, R.L., Crosser, O.K.: Thermal conductivity of heterogeneous two-component systems. Ind. Eng. Chem. Fundam. **1**(3), 187–191 (1962)
16. Zhang, X., Gu, H., Fujii, M.: Effective thermal conductivity and thermal diffusivity of nanofluids containing spherical and cylindrical nanoparticles. J. Appl. Phys. **100**(4), 044325 (2006)
17. Pantzali, M.N., Kanaris, A.G., Antoniadis, K.D., Mouza, A.A., Paras, S.V.: Effect of nanofluids on the performance of a miniature plate heat exchanger with modulated surface. Int. J. Heat Fluid Flow **30**(4), 691–699 (2009)
18. Geankoplis, C., Hersel, A., Lepek, D.: Transport Processes and Separation Process Principles, 5th edn. Pearson (2018)
19. Rehman, U.: Heat Transfer Optimization of Shell-and-Tube Heat Exchanger through CFD Studies (2011)

Modeling the Vapor-Liquid Equilibrium of CO_2-H_2O-$[C_NC_1Im][NTf_2]$ Blends Using Machine Learning Techniques to Determine Feasible Solvent Conditions for CO_2 Absorption in a Gas-Sweetening Unit

Ethan Zachary G. Castro[1,2](✉), Rhea Mae B. Biñar[1,2], Syla Y. Naval[1,2], and Bonifacio T. Doma Jr.[1,2]

[1] School of Chemical, Biological, and Materials Engineering and Sciences, Mapúa University, 1002 Muralla Street, Intramuros, Manila, Philippines
ezgcastro@mymail.mapua.edu.ph

[2] School of Graduate Studies, Mapúa University, 1002 Muralla Street, Intramuros, Manila, Philippines

Abstract. In the pursuit of sustainable development, ionic liquids (ILs) are of high research interest because of their properties, tuneability, and environmental-friendly features. One of the most notable applications of ILs is in CO_2 capture. Solvents with methylimidazolium-based cations partnered with the $[NTf_2]$ anion are being investigated due to their high affinity towards CO_2. However, these ILs are costly to synthesize and difficult to apply in industrial settings due to their high viscosity. As such, there is a need for pre-synthesis experiments and analysis. This study used machine learning techniques to predict the vapor-liquid equilibrium (VLE) of systems containing CO_2, H_2O, and $[C_NC_1Im][NTf_2]$. Data for $N = 1$ to $N = 4$ were generated using the PC-SAFT Equation of State and were then used to train independent models for CO_2 vapor composition and equilibrium pressure. The trained models could reliably predict the vapor's equilibrium composition and the equilibrium pressure for up to $N = 5$. Further, the machine learning models were used to solve a simple design problem, where an absorption tower used to sweeten the biogas produced from distillery press mud was considered. Solvent composition and the number of carbons yielding lower minimum solvent flow rate requirements were determined. It was found that high IL concentrations in the liquid and an increased number of carbons in the cation produced lower values for the minimum solvent flow rate required for the 99% separation of CO_2 from the inlet vapor.

Keywords: CO_2 Absorption · Ionic Liquids · Machine Learning · Methylimidazolium Cations · PC-SAFT Equation

C. Y. Chee and C. Wang (Eds.): ICMEN 2023, SPPHY 1068, pp. 20–37, 2024.
https://doi.org/10.1007/978-981-97-4080-2_2

1 Introduction

The global consumption of natural gas is projected to grow at an annual average of 0.8% from 2022 to 2025 [1]. This demand rise requires the use of raw natural gas contaminated with unwanted acids, which is classified as sour gas [2]. Sour gas usage causes numerous technical and operational issues, including equipment corrosion, deactivation of catalysts, fouling, and multiple ecological pollutions [3]. Hence, removing these acid contaminants from the sour gas is necessary to produce a purified gas known as sweet gas, which qualifies in pipeline specification requirements and is recognized as safe and efficient for several industrial applications [3, 4]. Removing acid contaminants, specifically hydrogen sulfide (H_2S) and carbon dioxide (CO_2), from the sour gas to produce a sweet gas containing less than 4 ppm of H_2S and 3% to 4% by mole of CO_2 is identified as the gas-sweetening process [5]. Currently, most gas-sweetening processes in large-scale industrial plants apply chemical absorption with the use of amine-based solvents, which include monoethanolamine (MEA), diethanolamine (DEA), and methyldiethanolamine (MDEA), absorbing agents [4]. However, the application of amine-based solvents in the gas-sweetening process poses several drawbacks, such as amine solvent degradation [6], formation of corrosive substances during amine degradation [7], low thermal stability [3], water transfer into the gas stream during desorption step, inadequate absorption capacity [6], and massive energy input during high-temperature absorbent regeneration by which the heat duty contributes up to 70% of the total operating cost of the absorption process [6, 8]. In addition, the increased energy input would require replacing existing columns with larger column diameters, increasing capital cost, which questions the economy of the overall process [3].

Recent studies suggest that ionic liquids (IL) as absorbents for CO_2 absorption and minor extension to H_2S overcome some of the issues faced in applying amine-based solvents in CO_2 capture and gas sweetening processes [6, 9]. ILs are known to be nonvolatile, stable even at elevated temperatures, have low heat capacity, have superior performance in dissolving CO_2 and H_2S, and have tunable chemistry, which means that properties can be tailored depending on the choice of either anion, cations, or other substituents [4, 6, 9–11]. Moreover, ILs have negligible vapor pressure, which assures that the gas stream is uncontaminated and that the loss of ILs due to evaporation would be insignificant [9, 11]. Among the ILs available, methylimidazolium-based ILs are mostly preferred in CO_2 capture and separations due to their superior compatibility with CO_2. This is because the acidic hydrogen atoms around the imidazole ring promote the solvation of CO_2 [12]. Partnered with the anion bis(trifluoromethylsulfonyl)imide [NTf_2], which possesses CO_2-philic fluoroalkyl groups and a large ionic radius [13], CO_2 indeed becomes highly soluble in [C_NC_1Im][NTf_2] ionic liquid solvents. However, ILs such as these can be costly to synthesize and can become highly viscous, especially during the absorption of CO_2, which limits their application in industrial processes [9].

Several studies have addressed this gap by taking advantage of the chemical tunability of ILs to tailor and modify their properties and satisfy the requirements of a specific application. Wappel et al. [11] designed and assessed eighty different ionic liquids and their blends and determined their CO_2 absorption performance compared with amine-based solvents. Experimental tests showed that pure ILs are inefficient in CO_2 absorption due to their highly viscous properties. Adding water lowered the viscosity of ILs, and